JOURNAL OF APPLIED POLYMER SCIENCE VOL. 14, PP. 2973–2998 (1970)

A Study of Fiber Extrusion in Wet Spinning. I. Experimental Determination of Elongational Viscosity

CHANG DAE HAN and LEON SEGAL, *Department of Chemical Engineering, Polytechnic Institute of Brooklyn, Brooklyn, New York 11201*

Synopsis

Elongational viscosities were measured in a wet-spinning apparatus. The advantage of this procedure lies in the fact that excellent temperature control can be maintained and that gravity effects can be neglected for a horizontally spun fiber. As a spin dope, an aqueous solution of polyacrylonitrile (PAN) consisting of approximately 10% polymer and 40% sodium thiocyanate (NaSCN) was spun into a coagulating bath of varying NaSCN content, up to a concentration at which spinning was no longer feasible. Fiber diameters were measured photographically as a function of distance from the spinnerette. Spinning tension readings were made on a multifilament bundle using a calibrated tensiometer. To eschew the influence of the hardening effect arising from mass and heat transfer, the temperatures of the spin dope and coagulating bath were kept constant, while the solvent concentration of the coagulating bath was varied up to a maximum limiting value. In this manner, the theoretical condition of no hardening is approached, and the experimentally determined elongational viscosity approaches a limiting, concentration-independent value. The rheological properties of the spin dope were determined independently in a jet thrust measurement device. Some of the experimentally determined results on elongational viscosity versus rate of elongation were presented and discussed in the light of the theoretical prediction based on various constitutive equations.

INTRODUCTION

Important polymer processes such as fiber spinning and film drawing involve "elongational flow" of the polymer melt or solution. For such a flow, determination of fluid "spinnability" is very important. Nitschmann and Schrade[1] appear to be the first who postulated that liquid systems can be spinnable only if they have a certain "anomalous" and characteristic viscosity behavior. This consists of an increase in viscosity with increased stretching rate, the so-called "apparent Trouton viscosity." According to Trouton,[2] who first introduced the concept, Trouton viscosity, η_T, is three times the Newtonian viscosity, η_0: $\eta_T = 3\eta_0$. However, much later it was pointed out by several investigators that this relation does not hold for many polymer substances, but is in fact a limiting condition at low stretching rates.

Recently, Ballman[3] carried out a study on the elongation of solid polystyrene rods. This study has been widely cited in the literature, although

only five data points for elongational viscosity are presented; Ballman states that elongational viscosity shows a maximum with respect to rate of elongation. Much earlier than Ballman, Kargin and Sogolova[4] investigated the extension of solid plastic rods and published results showing that elongational viscosity is in fact independent of elongation rate. Recently, Radyshkevich et al.[5] measured the elongational viscosity of polyisobutylene and also obtained a constant elongational viscosity. It must be noted that all the above experimental results involve elongation rates below 0.1 sec^{-1}, and the elongational behavior in this region cannot be extended into the region of higher elongation rates. In addition, the measurements were not performed at steady pulling speed, and so the results are of further limited value.

Ziabicki and Kedzierska[6] studied the elongation of a series of polymers by means of the melt-spinning process, and they found an increase of elongational viscosity along the spinning way. Ziabicki[7] studied the melt spinning of polycapronamide and measured the tensile force at various positions along the spinning way. He calculated the elongational viscosity η_E using the expression

$$\eta_E = T_{xx}/\frac{dV}{dx} \tag{1}$$

where T_{xx} is the axial tensile stress defined by the tension F per unit area at a position x, and dV/dx is the axial velocity gradient of a filament under stretching. The calculated elongational viscosity was shown to increase monotonically with distance along the spinning way. However, Ziabicki[7] could not separate the effects of the rate of elongation and temperature from the overall change of elongational viscosity, although temperature is one of the most influential factors in his experiment of melt spinning.

The cooling of the spun fiber increases elongational viscosity following the Eyring-Frenkel equation

$$\eta_E(T) = \eta_E(T_0)e^{E/R(1/T-1/T_0)} \tag{2}$$

in which $\eta_E(T)$ and $\eta_E(T_0)$ are the elongational viscosity at temperature T and T_0, respectively, E is the activation energy, and R is the gas constant. In a separate study, Ziabicki and Kedzierska[8] postulated that under the condition of constant tensile force the increase of elongational viscosity is a necessary condition for spinnability, so that an increase of axial velocity due to stretching had to be accompanied by an increase of elongational viscosity.

On the other hand, several authors analyzed the steady elongational flow of non-Newtonian viscoelastic fluids from the rheological point of view and succeeded in showing that elongational viscosity increases with the rate of elongation, whereas the non-Newtonian viscosity decreases with the rate of shear. To obtain this result, Yamamoto[9] used the network theory on a molecular basis, Lodge[10] used the integral form of Max-

wellian fluid, White[11] used a second-order fluid model, while Roscoe[12] used a third-order fluid model, both fluid models being special cases of the simple fluid theory advanced by Noll[13] and Coleman and Noll.[14] Bird and Spriggs[15] used the modified form of the three-constant Oldroyd model.[16]

It is the purpose of this paper to present some new experimental results on elongational viscosity. The results presented here were obtained by means of the wet-spinning process. The experimentally obtained results are compared with the theoretically predicted results.[10,15]

THEORETICAL BACKGROUND

An isochoric elongational flow may be defined by

$$v_i = a_i x_i \qquad i = 1,2,3 \tag{3}$$

where v_1 is the component of velocity in the direction of elongation of x_1, and v_2 and v_3 are the components of velocity in the x_2 and x_3 directions, which are perpendicular to the x_1 direction. From the equation of continuity we have

$$\sum a_i = a_1 + a_2 + a_3 = 0 \tag{4}$$

If we define

$$\frac{dv_1}{dx_1} = \bar{\gamma} \tag{5}$$

with $\bar{\gamma}$ being the steady elongation rate, the rate-of-elongational-strain tensor may be given by

$$\mathbf{e} = \begin{pmatrix} \bar{\gamma} & 0 & 0 \\ 0 & -\bar{\gamma}/2 & 0 \\ 0 & 0 & -\bar{\gamma}/2 \end{pmatrix}. \tag{6}$$

For any fluid, the total stress is given by

$$T_{ij} = -p\delta_{ij} + \tau_{ij}. \tag{7}$$

Now, if one defines the isotropic pressure p by

$$-p = {}^1/_3(T_{11} + T_{22} + T_{33}), \tag{8}$$

then the sum of the deviatoric stress component is given by

$$\tau_{11} + \tau_{22} + \tau_{33} = 0. \tag{9}$$

If the surfaces transverse to the direction of principal elongation are unconstrained,

$$T_{22} = T_{33} = 0 \tag{10}$$

and, from eq. (8),

$$-p = {}^1/_3\, T_{11} \tag{11}$$

Substituting eq. (11) into eq. (7) yields

$$T_{11} = {}^3/_2\, \tau_{11}. \tag{12}$$

From eqs. (7) and (10) the following is obtained:

$$p = \tau_{22} = \tau_{33}. \tag{13}$$

Substituting eq. (13) into eq. (7) yields an alternate expression for T_{11},

$$T_{11} = -\tau_{22} + \tau_{11}. \tag{14}$$

Equations (12) and (14) are two equivalent expressions for the total principal stress in an isochoric elongational flow.

Since the elongational viscosity η_E is defined as

$$\eta_E = \frac{-T_{11}}{\dot{\gamma}} \tag{15}$$

Use of eq. (12) in eq. (15) gives the following expression:

$$\eta_E = -{}^3/_2 \frac{\tau_{11}}{\dot{\gamma}}. \tag{16}$$

Use of eq. (14) in eq. (15) gives

$$\eta_E = \frac{\tau_{22} - \tau_{11}}{\dot{\gamma}}. \tag{17}$$

It is to be noted, however, that if the isotropic pressure p is not defined by eq. (8), which is quite arbitrary, in fact, eq. (16) does not have to be satisfied. This point will be made clear with specific constitutive equations.

The Three-Constant Oldroyd Model[16]

This model is given by

$$(1 + \lambda_1 \mathfrak{F}_0)\boldsymbol{\tau} = -2\eta_0(1 + \lambda_2 \mathfrak{F}_0)\mathbf{e} \tag{18}$$

where $\boldsymbol{\tau}$ is the stress tensor; $\mathbf{e}$ is the rate-of-strain tensor; λ_1, λ_2 are time constants ($\lambda_1 > \lambda_2$); η_0 is a zero-shear viscosity; and $\mathfrak{F}_0$ is a nonlinear differential operator defined by

$$\begin{aligned} \mathfrak{F}_0 \tau_{ik} &= \frac{\mathfrak{D}\tau_{ik}}{\mathfrak{D}t} - \tau_{ij}e_{jk} - \tau_{jk}e_{ij} + \frac{2}{3}\tau_{mj}e_{mj}\delta_{ik} \\ \mathfrak{F}_0 e_{ik} &= \frac{\mathfrak{D}e_{ik}}{\mathfrak{D}t} - 2e_{ij}e_{jk} + \frac{2}{3}e_{mj}e_{mj}\delta_{ik} \end{aligned} \tag{19}$$

where $\mathfrak{D}/\mathfrak{D}t$ is the Jaumann derivative defined by

$$\frac{\mathfrak{D}e_{ik}}{\mathfrak{D}t} = \frac{\partial e_{ik}}{\partial t} + v_m \frac{\partial e_{ik}}{\partial x_m} - \omega_{km}e_{mi} - \omega_{im}e_{mk}$$

in which ω_{im} is the vorticity tensor component defined by ${}^1/_2(e_{mi} - e_{im})$, and δ_{ik} is the Kronecker delta. Bird and Spriggs[15] have derived expressions for τ_{11} and τ_{22} for steady elongational flow using this model:

$$\tau_{11} = -2\eta_0\left(\frac{1-\lambda_2\bar{\gamma}}{1-\lambda_1\bar{\gamma}}\right)\bar{\gamma} \tag{20}$$

$$\tau_{22} = \eta_0\left(\frac{1-\lambda_2\bar{\gamma}}{1-\lambda_1\bar{\gamma}}\right)\bar{\gamma} \tag{21}$$

Use of eq. (20) into eq. (16) gives the following:

$$\eta_E = 3\eta_0\left(\frac{1-\lambda_2\bar{\gamma}}{1-\lambda_1\bar{\gamma}}\right) \doteq 3\eta_0[1 + (\lambda_1 - \lambda_2)\bar{\gamma}]. \tag{22}$$

It is readily seen that eq. (17) is also satisfied.

The Spriggs Four-Constant Model[17]

This model is given by

$$(1 + \lambda_p\mathfrak{F}_\epsilon)\boldsymbol{\tau}^p = -2\eta_p\mathbf{e}^p \tag{23}$$

where $\eta_p = \eta_0\left(\lambda_p/\sum_{p=1}^{\infty}\lambda_p\right)$; the total $\boldsymbol{\tau}$ and $\mathbf{e}$ are given by $\sum_{p=1}^{\infty}\boldsymbol{\tau}^p$ and $\sum_{p=1}^{\infty}\mathbf{e}^p$, respectively; and the nonlinear operator $\mathfrak{F}_\epsilon$ is defined by

$$\mathfrak{F}_\epsilon e_{ik} = \frac{\partial}{\partial t}e_{ik} + v_m\frac{\partial e_{ik}}{\partial x_m} + \frac{1}{2}(\omega_{im}e_{km} + \omega_{km}e_{im}) - (1+\epsilon)\left[(e_{ij}e_{jk}) - \frac{1}{3}e_{mj}e_{mj}\delta_{ik}\right]. \tag{24}$$

The fourth constant, ϵ, may be taken as zero with no loss of generality if the Weissenberg hypothesis is assumed, i.e., the second normal stress difference is zero. For steady elongational flow, we then have

$$\tau_{11} = \frac{-2\eta_p\bar{\gamma}}{(1-\lambda_p\bar{\gamma})} \tag{25}$$

$$\tau_{22} = \frac{\eta_p\bar{\gamma}}{(1-\lambda_p\bar{\gamma})} \tag{26}$$

and use of eq. (25) in eq. (16) yields

$$\eta_E = 3\frac{\eta_p}{(1-\lambda_p\bar{\gamma})} = \frac{3\eta_0}{Z(\alpha)}\sum_{p=1}^{\infty}\frac{1}{p^\alpha(1-\lambda_p\bar{\gamma})} \tag{27}$$

where $Z(\alpha)$ is the Riemann zeta function. For the simplest case, $p = 1$, eq. (27) reduces to

$$\eta_E = \frac{3\eta_0}{(1-\lambda_1\bar{\gamma})} \doteq 3\eta_0(1 + \lambda_1\bar{\gamma}) \tag{28}$$

which is similar in form to eq. (22). Use of eq. (17) gives the identical result as eq. (28). Therefore, we have shown that at least these two differential-type constitutive equations give rise to consistent expressions for elongational viscosity, either from eq. (16) or eq. (17). It is to be

noted, however, that the isotropic pressure p is defined in both constitutive equations, eqs. (18) and (23), by eq. (8).

Lodge's Elastic Liquid Model[10]

This model is given by

$$\tau = -\int_0^\infty m(\tau')\mathbf{C}^{-1}(\tau')d\tau' \tag{29}$$

where $m(\tau')$ is a memory function, which according to Lodge[10] can be taken as

$$m(\tau') = \sum_{n=1}^{\infty} \frac{\eta_0}{\lambda_n^2} e^{-\tau'/\lambda_n}, \tag{30}$$

and $\mathbf{C}^{-1}(\tau')$ is the strain tensor, which is defined in steady elongational flow by

$$\mathbf{C}^{-1}(\tau') = \begin{pmatrix} e^{2\bar{\gamma}\tau'} & 0 & 0 \\ 0 & e^{-\bar{\gamma}\tau'} & 0 \\ 0 & 0 & e^{-\bar{\gamma}\tau'} \end{pmatrix} \tag{31}$$

in which τ' is the elapsed time, defined by

$$\tau' = t - t' \qquad 0 \leq \tau' < \infty \tag{32}$$

where t is the present time and t' is the past time.

Solving eq. (29) for τ_{11} and τ_{22} gives, for $n = 1$ in the memory function, as presented by Lodge,[10]

$$\tau_{11} = \frac{\eta_0}{\lambda_1(2\lambda_1\bar{\gamma} - 1)} \tag{33}$$

$$\tau_{22} = \frac{-\eta_0}{\lambda_1(\lambda_1\bar{\gamma} + 1)} \tag{34}$$

Substitution of eq. (33) into eq. (16) gives, with $2\bar{\gamma}\lambda_1 < 1$,

$$\eta_E = \frac{3}{2}\frac{\eta_0}{\lambda_1\bar{\gamma}(1 - 2\lambda_1\bar{\gamma})} \doteq 3\eta_0\left(1 + \frac{1}{2\lambda_1\bar{\gamma}}\right). \tag{35}$$

On the other hand, use of eqs. (33) and (34) in eq. (17) gives

$$\eta_E = \frac{3\eta_0}{(\lambda_1\bar{\gamma} + 1)(1 - 2\bar{\gamma}\lambda_1)} \doteq 3\eta_0(1 + \lambda_1\bar{\gamma}), \tag{36}$$

which is not identical with eq. (35). However, one should note that in eq. (29) the isotropic pressure p is not defined by eq. (8) and that use of eq. (16) to derive the expression for elongational viscosity is not justified. Therefore, eq. (35) is not a correct expression for elongational viscosity, using such constitutive equations as eq. (29), and hence only eq. (36) remains correct.

A recent summary by Bird et al.[18] compares the various expressions for elongational viscosity η_E derived from network theories of concentrated

solutions, suspension theories, and continuum models. While most theories predict η_E increasing to infinity, a network "rupture" model by Tanner and Simmons[19] predicts η_E increasing to a maximum and then decreasing indefinitely, while a molecular theory by Bird et al.[18] predicts an increase and then a decrease to an asymptotic value. Unfortunately, neither Tanner's nor Bird's model lends itself easily to comparison to experimental results because of certain difficulties in determining the model parameters. Thus, the simplest models appear to remain the most useful, if not (as will be shown) the most rigorously correct.

EXPERIMENTAL

In the present study, an attempt was made to experimentally determine the dependence of elongational viscosity on elongation rate in terms of the rheological properties of the fluids tested. As an experimental device, the fiber wet-spinning process was chosen.

Apparatus and Procedure

A schematic representation of the spinning apparatus is shown in Figure 1. Compressed gas forces the spinning solution into the Zenith variable-speed metering pumps. The flow rate to the spinnerette is the differential flow from two such positive displacement pumps operating at slightly different speeds. This arrangement allows for good flow control at extremely low flow rates and for rapid initial filling of the system. The spinnerettes used are made of precious metal alloys. The emerging filaments are passed through the coagulating bath, and the fiber is then led over the pulleys of a tensiometer and on to the variable speed take-up roll. Measurements of thread tension are made at various values of jet stretch (the ratio of take-up velocity to plug flow spinnerette velocity,

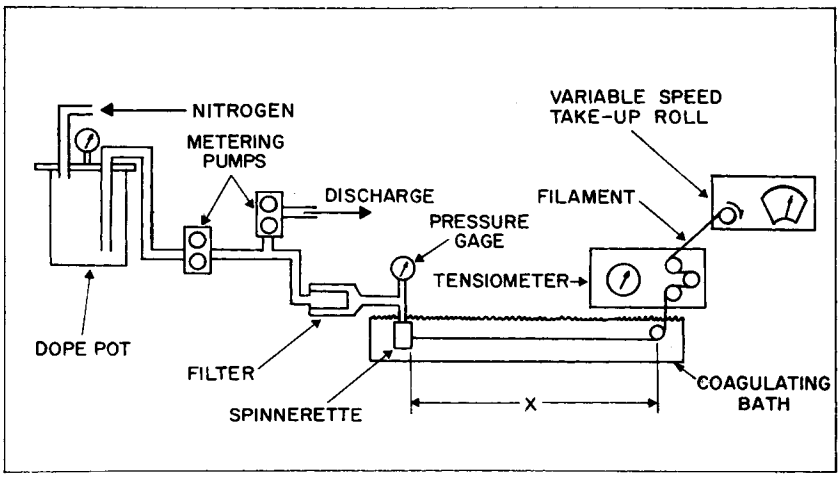

Fig. 1. Schematic representation of the spinning apparatus.

V_2/V_1), keeping the shear rate in the spinnerette hole constant. In, practice, multihole spinnerettes were used for tension measurements, since the tension per filament is quite low and this procedure gave measurable and accurate tension readings to values below 0.05 g per filament. Spinnerette diameters of 0.005 in. (0.0130 cm), 0.012 in., and 0.015 in. were used. Filament diameter was measured photographically as a function of the distance from the spinnerette face, using a three-hole spinnerette.

The Spinning Systems and Spinning Conditions

The material used was a proprietary fiber-forming dope similar to standard commercial dopes: an aqueous polymer solution consisting of approximately 10% polyacrylonitrile (PAN) and 40% sodium thiocyanate (NaSCN). The polymer molecular weight was approximately 100,000, and the specific gravity was 1.30 at 30°C. The coagulating bath ranged in concentration from 0% through 25% NaSCN in water at a temperature of 20°C. Experiments were performed at temperatures of 0°C, 20°C, and 40°C at a bath concentration of 10% NaSCN. The jet stretch (V_2/V_1) was varied up to the point at which the thread broke down. Free velocity measurements were also taken by photographing the diameter of a freely extruded filament at the above concentrations and temperatures.

Rheological Characterization of Spinning Solutions

To "theoretically" predict the elongational or shear behavior of a fluid, the material constants of a chosen constitutive equation must be determined. This was accomplished by experimentally determining the shear and/or normal stresses and then evaluating the material constants so as to obtain the best fit between the theoretical and experimental curves. In this study, both shear stress and normal stress differences at the high shear rates (10^2 to 10^4 sec^{-1}) encountered in fiber spinning were measured by a jet thrust apparatus as described by Shertzer.[20] This apparatus determines stresses at high values of shear rate by measurement of the thrust (reaction) of a free, horizontal jet. Furthermore, the viscosity at these shear rates was simultaneously determined since the instrument is, in effect, a suspended capillary rheometer.

RESULTS AND DISCUSSION

Tension Measurements

In the wet spinning of fibers, the total measured takeup force, F_{tot}, is actually the sum of several forces the primary components of which are the rheological force, F_{rheo}, and the drag force, F_{drag}. F_{rheo} is the force required for the deformation of a thread, and it is related to the axial stress component, p_{xx}, and to the elongational viscosity, η_E, through the following equation:

$$F_{rheo}/A(x) = p_{xx}(x) = \eta_E dV(x)/dx \tag{37}$$

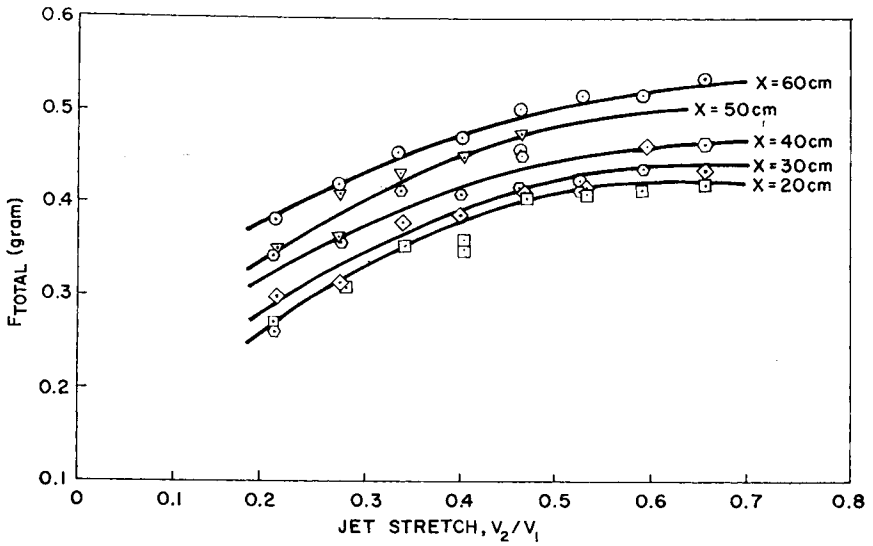

Fig. 2. F_{tot} vs. jet stretch. Bath concn. = 10% NaSCN; bath temp. = 20°C; V_1 = 16.62 cm/sec.

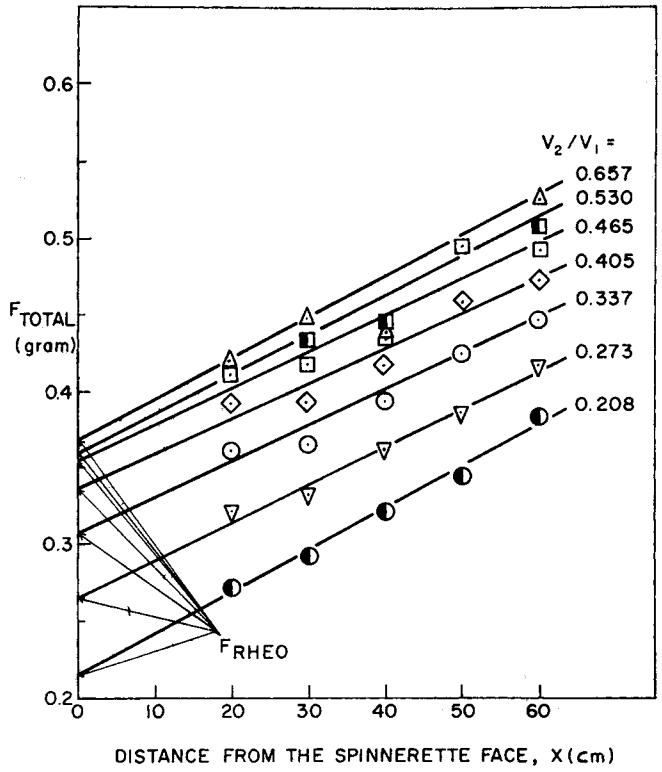

Fig. 3. F_{tot} vs. distance (cm) from the spinnerette face. Bath concn. = 10% NaSCN; bath temp. = 20°C; V_1 = 16.62 cm/sec.

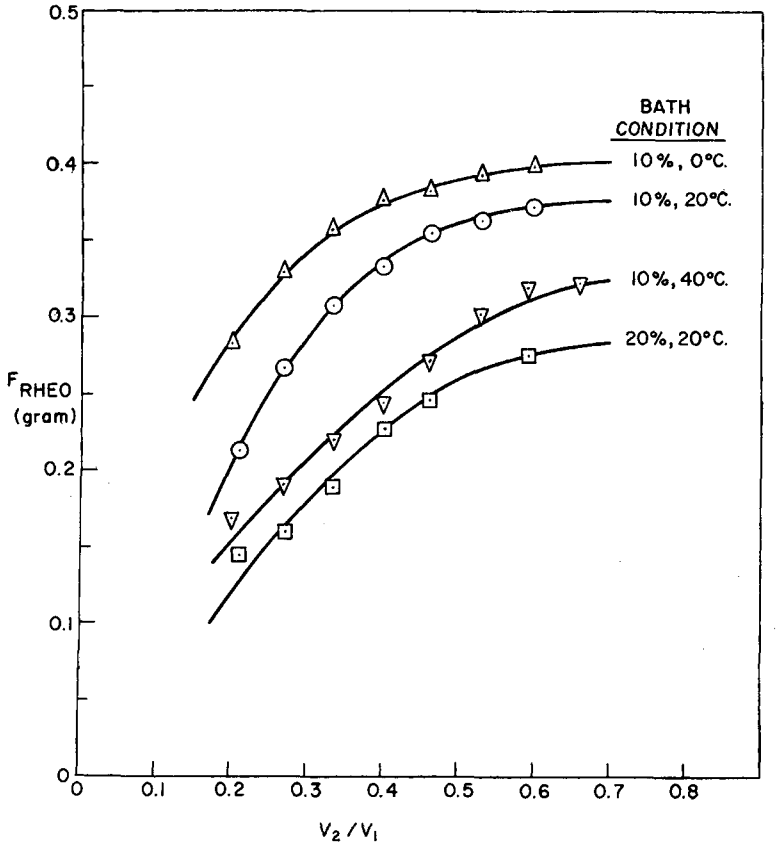

Fig. 4. F_{rheo} vs. jet stretch at different bath conditions. Spinnerette diam. = 0.005 in.; V_1 = 16.62 cm/sec.

where $dV(x)/dx$ is the axial velocity gradient and $A(x)$ is the cross-sectional area of the thread. It is seen that F_{rheo} exists only in the region where the deformation process occurs, i.e., where the value of the axial velocity gradient is non-zero. Furthermore, F_{rheo} is considered to be constant through the length of the fiber in which it is defined, while F_{drag} is considered to be dependent on distance x from the spinnerette face. Physically, F_{rheo} is an internal force, while F_{drag} is an external force. F_{drag} has been measured by Griffith,[21] but his expressions for F_{drag} cannot be generalized for all systems.

Other less important components of F_{tot} (at least in the wet-spinning process) are: the force due to gravity, the kinetic energy force due to the accelerating mass of filament, and surface tension forces. These force components are significant only in the melt or dry-spinning processes. These forces are also "external" forces and can be lumped together with F_{drag} in the following force balance equation:

$$F_{tot}(x) = F_{rheo} + F_{coag}(x) \tag{38}$$

where F_{coag}, which we call the coagulating force, is the sum of all these external force components.

It is seen from eq. (37) that the force of interest in the determination of elongational viscosity is F_{rheo}. Since $F_{coag}(x)$ is equal to 0 at $x = 0$ (at or near the spinnerette face), the numerical value of F_{tot} evaluated at $x = 0$ is essentially F_{rheo}. Determination of F_{tot} at several values of x and extrapolation of F_{tot} versus x curves to the ordinate intercept (at $x = 0$) thus yields the value of F_{rheo}.

Curves of F_{tot} versus V_2/V_1 (jet stretch) at various values of x (the takeup roll position) are presented in Figure 2 for a spinning condition in which the bath concentration is 10% NaSCN and the bath temperature is 20°C. The cross plots, F_{tot} versus x, at constant values of V_2/V_1, are shown in Figure 3. It is seen from Figure 2 that F_{tot} increases with jet stretch at all values of x and approaches a limiting value near the maximum (break-up) velocity. Figure 3 shows that F_{tot} increases with x, and the slope of the family of lines is fairly constant. This slope is directly related, of course, to the magnitude of the coagulation force, F_{coag}.

In any case, the quantity of primary concern to us here is F_{rheo}, which can be obtained from the intercept of the F_{tot} versus x curves in Figure 3 at $x = 0$. The procedures presented in Figures 2 and 3 are repeated for every set of spinning conditions, and the summary of the results for F_{rheo} versus V_2/V_1 are presented in Figure 4 for a spinnerette diameter of 0.005 in. The effect of spinnerette diameter upon filament tension and tensile

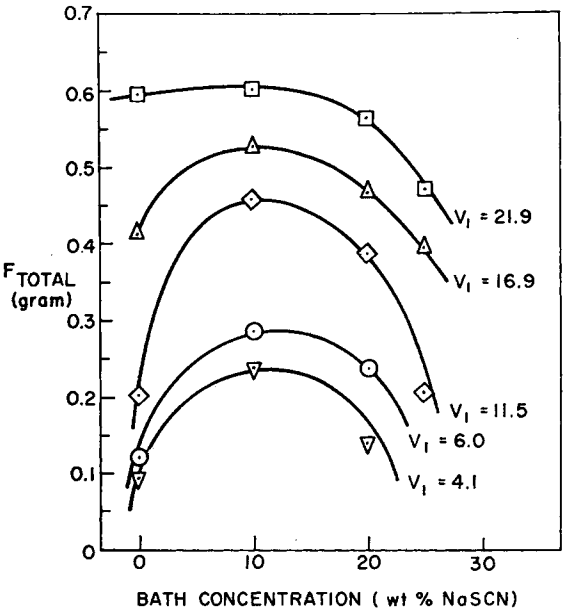

Fig. 5. F_{tot} vs. coagulating bath concentration at jet stretch V_2/V_1 of 0.6; $x = 65$ cm; $T = 20$°C.

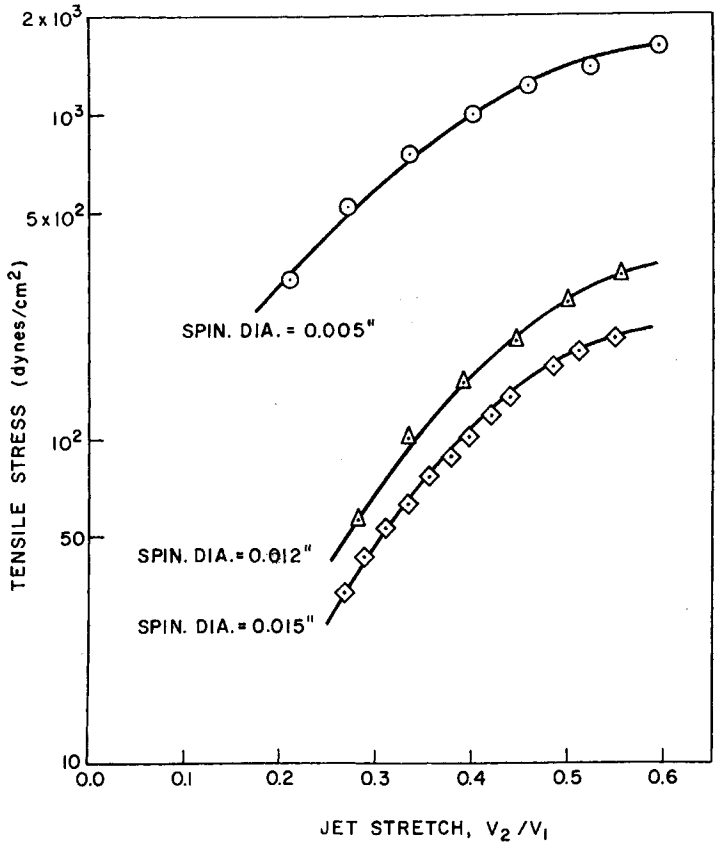

Fig. 6. Tensile stress vs. jet stretch. Bath concn. = 10% NaSCN; bath temp. = 20°C; $\dot{\gamma} = 10^4$ sec^{-1}.

stress will be discussed below. It is seen from Figure 4 that F_{rheo} increases as temperature decreases from 40°C to 0°C. It was also observed that F_{rheo} decreases as the batch concentration increases in the range 10% to 20%. It is expected that tension increases with decreasing bath temperature since it becomes more difficult (i.e., requires a higher tension) to draw a viscous substance at low temperatures than at high temperatures. While the bath temperature, not the dope temperature, is actually the variable, the small fiber dimensions allow us to assume that the fiber itself is probably at or near the bath temperature upon emergence from the spinnerette.

It may be expected that F_{rheo} continually decreases as the bath concentration increases, owing to the slower rate of coagulation. However, this expectation was not justified in actual experiment. The dependence of total tension F_{tot} on bath concentration is given in Figure 5 for bath concentrations of 0% through 25% and spinnerette diameter 0.005 in. (Total tension rather than F_{rheo} is presented here, only because actual data

points are available for the former quantity. As shown above, the behavior of these two quantities is always qualitatively similar.) It is seen from Figure 5 that tension goes through a maximum with respect to bath concentration in the vicinity of 10% NaSCN. This is extremely interesting since it is known that commercial spinning of this type of polymer–solvent–bath system is usually performed at a comparable bath concentration and at low temperatures.[22,23]

The effect of spinnerette hole diameter upon F_{rheo} can best be seen in a plot of tensile stress ($4F_{rheo}/\pi D_2^2$) versus jet stretch, with spinnerette diameter as a parameter. Here, D_2 is the diameter of the filament at the take-up roll. Assuming a constant density fluid, D_2 is calculated from the following equation:

$$D_2 = (4Q/\pi V_2)^{1/2} \tag{39}$$

where Q is the volumetric flow rate through the spinnerette and V_2 is the velocity at the takeup roll.

Figure 6 shows the important effect of spinnerette hole diameter upon tensile stress. It is seen that as the diameter increases from 0.005 to 0.015 in., the tensile stress decreases by a factor of approximately 10. This is due to the fact that the tensile stress depends, of course, upon the square of the filament diameter. It is also interesting to note that the three curves of Figure 6 are of very similar shape.

It should be noted from the above results that the jet stretch V_2/V_1 is in most cases less than unity, indicating apparently that the take-up velocity is less than the throughput velocity. However, if, instead of V_1, one uses the free jet velocity V_f, which is always lower than the throughput velocity V_1, the jet stretch V_2/V_f becomes larger than unity. The free jet velocity V_f can be calculated from the measurement of the free jet diameter D_f by

$$V_f = V_1(D_1/D_f)^2 \tag{40}$$

where D_1 and D_f are the diameters of the spinnerette hole and the free jet, respectively. Since D_f is larger than D_1 due to extrudate swelling, the free jet velocity V_f is smaller than the throughput velocity V_1. An alternative way of interpreting the results, in terms of the jet stretch defined by V_2/V_f instead of V_2/V_1, will be extensively discussed in connection with the problems associated with "fiber spinnability" in part II of the series.

Diameter Measurements

Fiber diameter versus distance is shown in Figure 7 for two values of spinnerette diameter. Since the shear rate in the spinnerette is kept constant, the throughput velocity V_1 is increased proportionately to the spinnerette hole diameter according to the following equation:

$$\dot{\gamma} = 4Q/\pi R^3 = 8V_1/D_1 \tag{41}$$

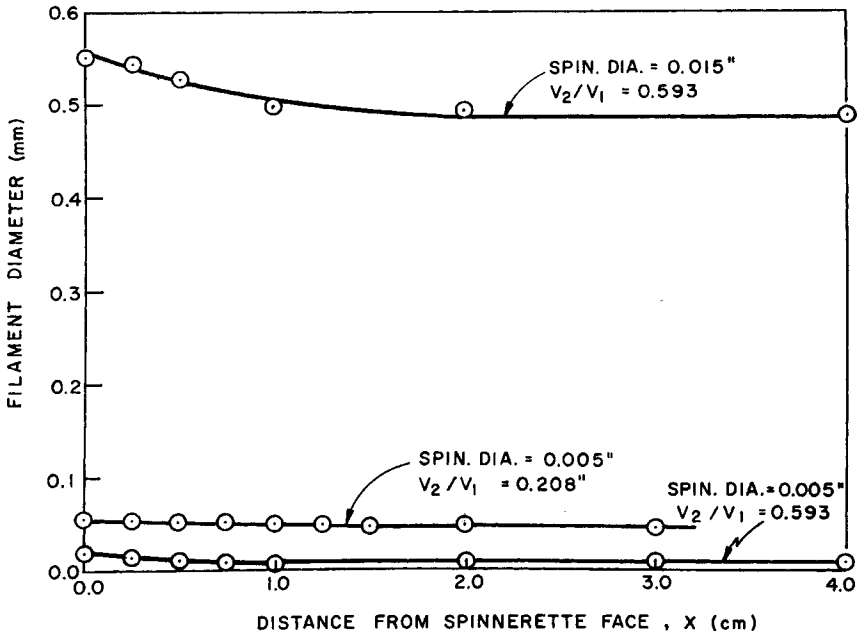

Fig. 7. Fiber diameter vs. distance (cm) from the spinnerette face. Bath conditions same as in Fig. 6; $\dot{\gamma} = 10^4$ sec^{-1}.

where $\dot{\gamma}$ is the shear rate at the wall of the spinnerette capillary. It is seen from Figure 7 that diameter decreases with distance and with take-up velocity, as expected. It is also seen that the change in diameter with distance is greater for larger V_2/V_1 and is greater for larger spinnerette diameters.

For a constant density filament, the axial velocity of the filament, $V(x)$, is related to the diameter $D(x)$ at any position x by

$$V(x) = 4Q/\pi D(x)^2 \tag{42}$$

and hence, the velocity gradient, dV/dx, is obtained as follows:

$$\frac{dV(x)}{dx} = \frac{-8Q}{\pi D(x)^3}\frac{dD(x)}{dx} \tag{43}$$

where Q is the volumetric flow rate. Thus, diameter measurements as a function of the position x yield the axial velocity and its gradient as functions of position x.

Figure 8 shows, as does Figure 7, that larger elongation rates can be expected as jet stretch V_2/V_1 increases and as the spinnerette hole diameter increases. Curves at different (intermediate) values of jet stretch lie within the envelope formed by the two given curves. The same relations apply at different bath concentrations (and temperatures), although the absolute value of filament diameter is a function of the bath concentration, since a higher bath concentration allows more swelling of the filament.

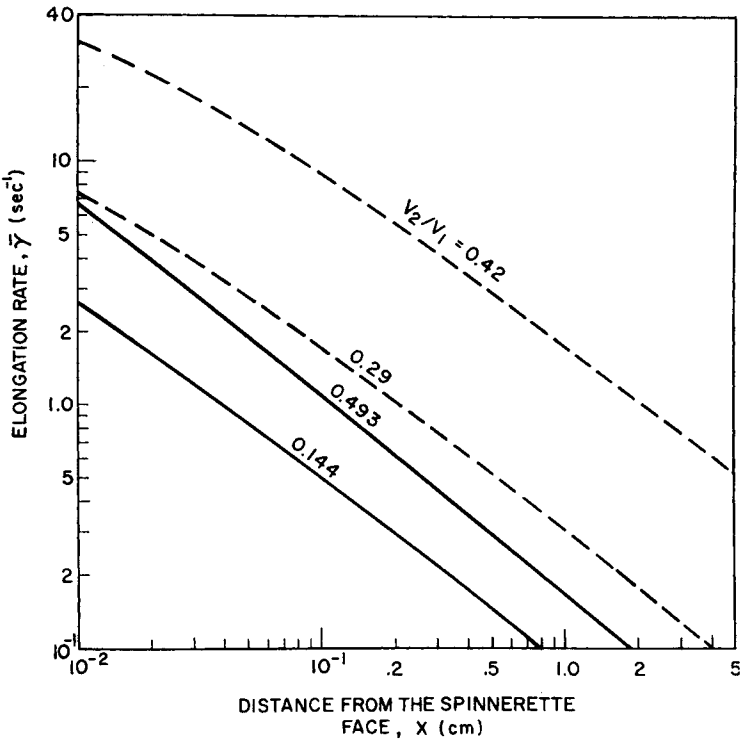

Fig. 8. Rate of elongation vs. distance (cm) from the spinnerette face. Bath conditions same as in Fig. 6; $\dot{\gamma} = 1.02 \times 10^4$ sec^{-1}; solid lines for 0.005 in. spinnerette diameter; dashed lines for 0.015 in. spinnerette diameter.

Effect of Bath Concentration on Free Jet Diameter

The diameter of a freely extruded filament, which has been mentioned previously in a discussion of the free velocity, is very important in the determination of the diameter of the filament under tensile stress. In general, it may be expected that the larger the free diameter, the larger will be the drawn diameter of the thread. This free diameter is strongly dependent upon the coagulating bath conditions for a given throughput rate.

It is known that "skin" formation is extremely important in the wet-spinning process, since the rigid "skin" acts as a solid boundary which limits the degree of jet swell.[22–24] Furthermore, the rate of "skin" formation, which is primarily determined by the coagulating bath concentration, is important because a rapid rate of coagulation actually impedes further coagulation of the fluid core of the filament.

Figure 9 is a plot of free jet swell ratio (D_f/D_1) versus bath concentration for three spinnerette diameters. As the concentration of the coagulating bath increases from 0% NaSCN (pure water), the free jet diameter increases. This, of course, is caused by the decrease in the rate of coagulation which

allows greater jet expansion. However, at a certain value of bath concentration (20% NaSCN for this system, independent of spinnerette diameter), the free diameter begins to decrease as the bath concentration is further increased. It may be surmised that at these high concentrations and hence at low rates of coagulation, "skin" formation is inhibited and the entire extruded filament swells into a gel-like structure. The degree of swelling of the gel is controlled by the solvent–polymer interaction, and

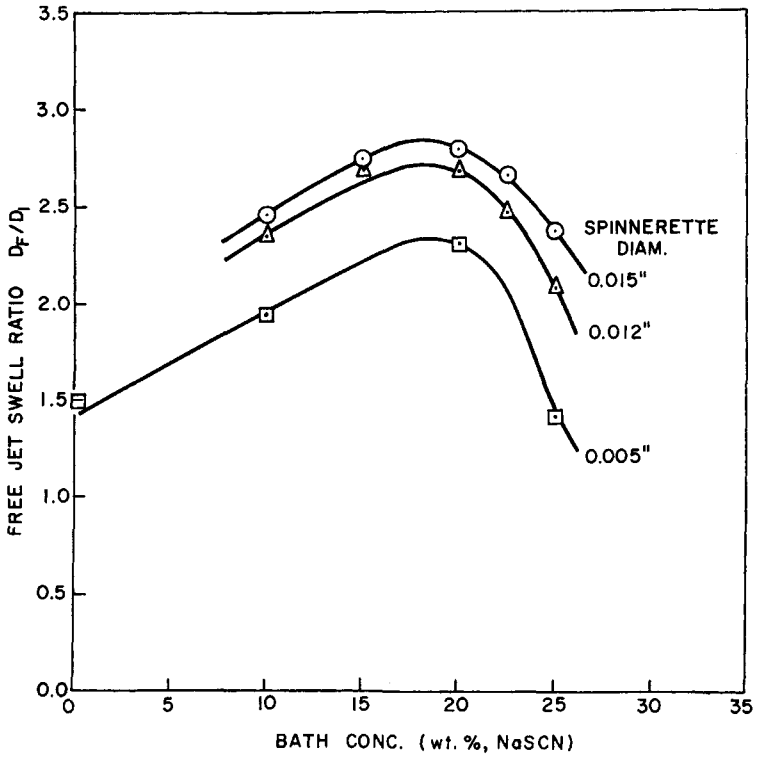

Fig. 9. Free jet swell ratio vs. bath concentration. Bath temp. = 20°C; $\dot{\gamma} = 10^4$ sec^{-1}.

therefore this behavior cannot be generalized for all systems. This would then explain the rather surprisingly low values of D_f/D_1 for 25% NaSCN in Figure 9.

Since the critical value of bath concentration is independent of spinnerette size, and since the free jet swell ratio D_f/D_1 is a measure of the degree of coagulation, minimum "hardening" is assumed to occur at the maximum of D_f/D_1 with respect to concentration. For our system, therefore, "true" hardening is effectively minimized at 20% bath concentration, rather than at higher bath concentrations.

Experimentally Determined Behavior of Elongational Viscosity

At a given set of operating conditions, i.e., throughput rate, take-up velocity, bath temperature, and concentration, the value of F_{rheo} is uniquely determined, and values of tensile stress, $p_{xx} = F_{\text{rheo}}/A(x)$, as a function of distance x can also be determined from the measurement of fiber diameter (see Fig. 8). The values of tensile stress p_{xx} and rate of elongation dV/dx at any fixed position x are easily calculable, and the quotient is equal to the elongational viscosity, according to eq. (37). Elongational viscosities very close to the spinnerette face are presented in Figures 10 and 11 for a hole diameter of $D_1 = 0.005$ in. The effects of bath concentration on elongational viscosity are shown in Figure 10, and the effects of bath temperature on elongational viscosity are shown in Figure 11. The values of elongational viscosity at the spinnerette face (i.e., $x = 0$) correspond to the point where hardening effects are minimized, and so the elongational viscosities at this position should be the lowest in magnitude. Furthermore, the results show that the magnitude of elongational viscosity decreases as bath concentration increases (Fig. 10) and increases as bath temperature decreases (Fig. 11). The effect of bath temperature on

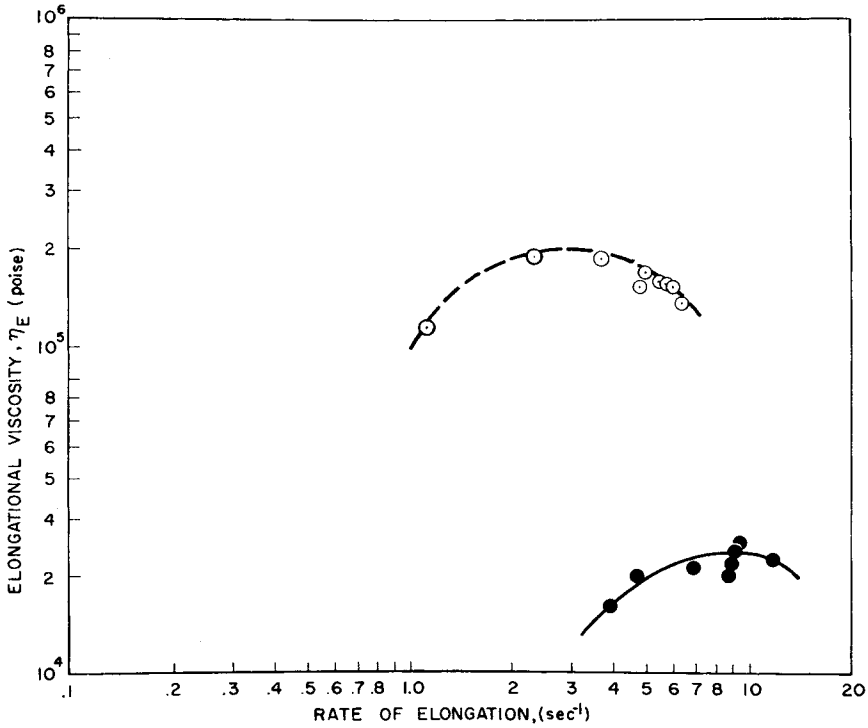

Fig. 10. Elongational viscosity vs. rate of elongation at different bath concentrations (10% and 20% NaSCN). Spinnerette diameter = 0.005 in.; dashed curve for 10% NaSCN; solid curve for 20% NaSCN; bath temp. = 20°C.

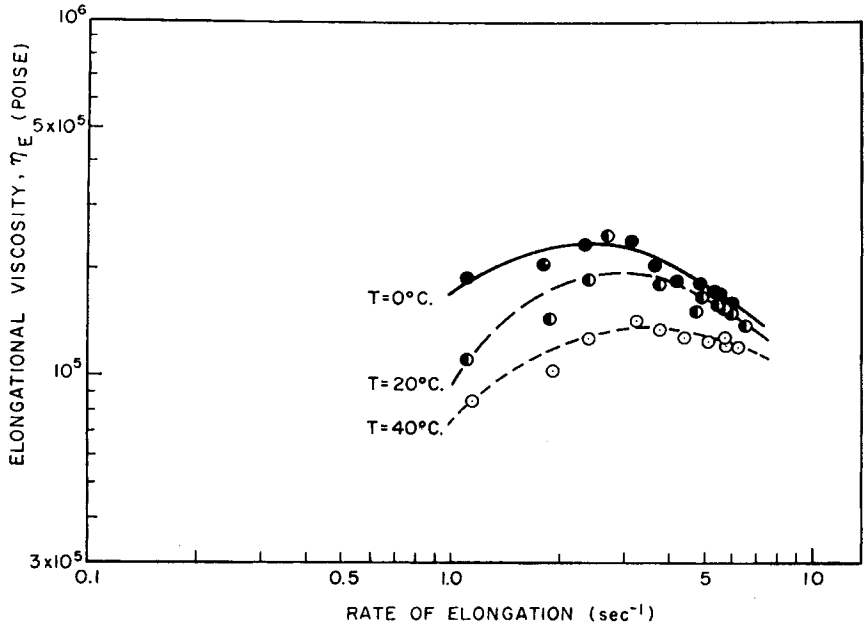

Fig. 11. Elongational viscosity vs. rate of elongation at different bath temperatures (0°C, 20°C, and 40°C). Spinnerette diameter = 0.005 in.; bath concn. = 10% NaSCN.

elongational viscosity η_E is perhaps better seen in Figure 12, where η_E is plotted against $1/T$ (°K^{-1}), with jet stretch as parameter. The slope of the lines in Figure 12 is proportional to the "activation energy" E of the Eyring-Frenkel equation, eq. (2). It should be noted here that E is seen to be a function of the bath conditions and rate of elongation, since jet stretch is a direct function of rate of elongation. The values of E at given bath conditions are shown in Table I. Referring again to Figures 10 and 11, the behavior of elongational viscosity follows a pattern very similar to the data of Ballman,[3] i.e., the curves go through a maximum in all cases. It is to be noted that Ballman investigated the elongational viscosity for rates of elongation ranging from 10^{-3} to 10^{-2} sec^{-1}.

TABLE I
Activation Energy of Polyacrylonitrile Solution in Elongational Flow[a]

Jet stretch V_2/V_1	Activation energy, cal/mole
0.201	28.2
0.273	26.1
0.465	13.7
0.657	7.56

[a] Coagulating bath conditions are 10% NaSCN and at 20°C.

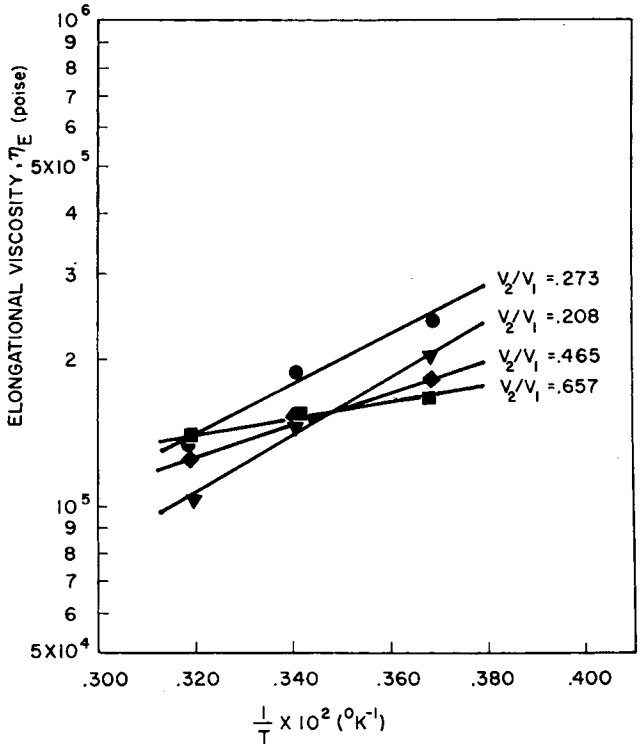

Fig. 12. Elongational viscosity vs. temperature. Bath concn. = 10% NaSCN.

It has been shown that both the tensile stress and rate of elongation are dependent upon the spinnerette hole diameter and the bath concentration. It would therefore be expected that the elongational viscosity is also highly dependent upon these variables. From Figure 9 one can assume that the degree of hardening is effectively minimized at a bath concentration of approximately 20% NaSCN. It is therefore desirable to evaluate the elongational viscosity for different spinnerette hole sizes at this condition of "minimum hardening."

The determination of filament tension for spinnerettes of large diameter (0.012 and 0.015 in.) at a bath concentration of 20% NaSCN was found to be very difficult because at this concentration tension readings are too low to be measured accurately (see Fig. 5). This problem was circumvented by measuring the tension (and calculating F_{rheo}) at four different bath concentrations: 10%, 14%, 15%, and 16% NaSCN, and then extrapolating these values to 20% NaSCN bath concentration. Figure 13 is a plot of F_{rheo} versus V_2/V_1 for spinnerette diameters 0.012 and 0.015 in., showing curves plotted from measured values (bath concentration 10% to 16% NaSCN) and then extrapolated to 20% NaSCN. The extrapolation procedure consists of crossplotting tension as a function of concentration; these curves are not presented here. In the calculation of elongational

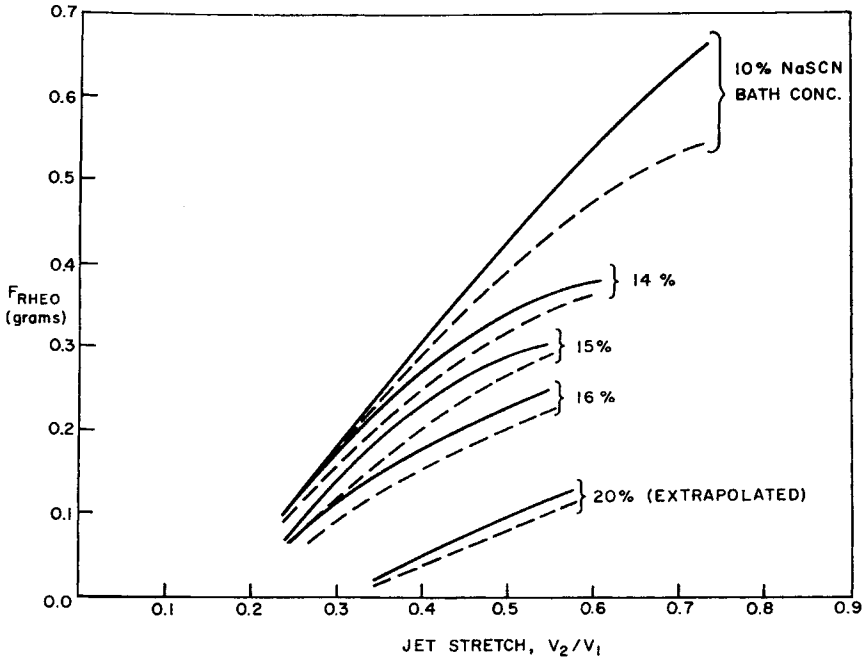

Fig. 13. F_{rheo} vs. jet stretch for different bath concentrations (14%, 15%, and 16% NaSCN). Bath temp. = 20°C; $\dot{\gamma} = 10^4$ sec^{-1}; solid curves for 0.015 in. spinnerette diameter; dashed curves for 0.012 in. spinnerette diameter.

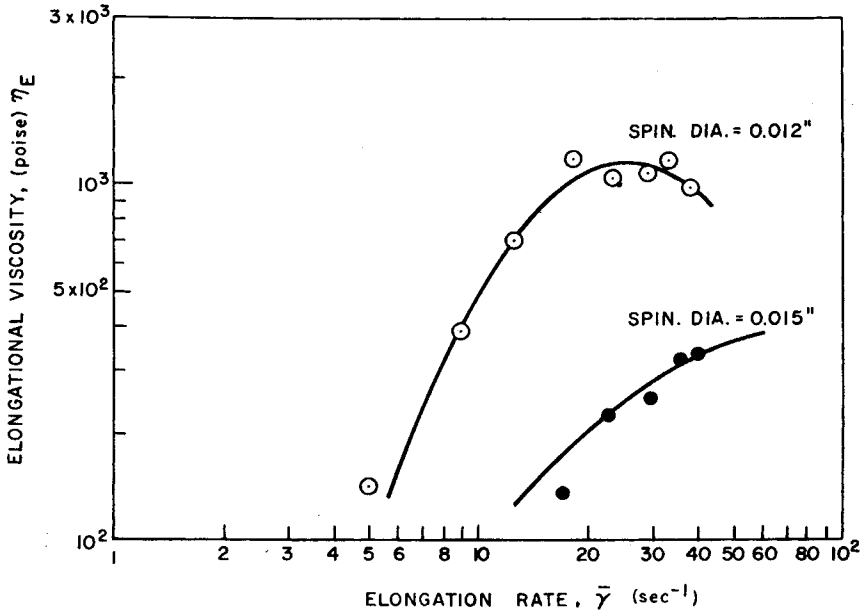

Fig. 14. Influence of spinnerette hole size on elongational viscosity. Bath concn. = 20% NaSCN; bath temp. = 20°C; $\dot{\gamma} = 10^4$ sec^{-1}.

viscosity at 20% NaSCN bath concentration, the extrapolated curves of Figure 13 will be used.

Figure 14 is a plot of elongational viscosity versus rate of elongation for spinnerette hole diameters of 0.012 and 0.015 in. and for the bath concentration of 20% NaSCN. The shape of these curves is very similar to those of Figure 10, while the magnitudes of their respective elongational viscosities are quite different. This is due to the fact that as the spinnerette hole diameter increases, the tensile stress decreases but the rate of elongation increases. Therefore, the ratio of tensile stress to rate of elongation (i.e., elongational viscosity) then decreases as the spinnerette hole size is increased.

A further interesting observation may be made about the effect of spinnerette diameter upon elongational viscosity. Clearly, any basic rheological property such as elongational viscosity should not be dependent upon the geometry of the system used to measure it. However, in the case of wet spinning, this geometry dependence may be misleading since we are actually using the spinnerette hole size as a means of controlling hardening. As may be expected, the increase in the spinnerette hole size decreases the influence of coagulation. In the absence of hardening, the elongational viscosity should be independent of spinnerette hole size.

Theoretically Predicted Behavior of Elongational Viscosity

In order to compare the experimentally determined elongational viscosity with the theoretically predicted one, one first has to determine the material constants in a given constitutive equation. For this purpose, we have chosen the jet thrust instrument of Shertzer,[20] because the shear rates in the spinnerette hole in our experimental work lie somewhere between 5×10^3 and 2×10^4 sec^{-1}. Because of the highly viscoelastic nature of the spinning dope used for this study, the capillary length-to-diameter ratio was limited to about 100 rather than the recommended 200. Reynolds numbers ranged between 0.3 and 90, while the recommended minimum is above 100 according to Shertzer.[20] In addition, previous thrust measurements were reported between 0.1 and 20 g, while in these experiments thrusts of from 12 to 100 g were measured. In view of these conditions, it appears that this apparatus is not ideal for measurement of normal stress in highly concentrated (highly viscoelastic) solutions, unless some modification is made.

The shear and normal stress curves are shown in Figure 15 and the viscosity curve is shown in Figure 16. Only normal stresses corresponding to Reynolds numbers greater than 15 are shown, and the curve is evidently of limited usefulness. The shear stress and viscosity measurements, on the other hand, are not subject to any of the above restrictions, and these curves are much more precise. It is seen that the region of interest, i.e., $\dot{\gamma} = 10^3$–10^4 sec^{-1}, is well in the power law region of flow. In the present study, Figure 16 is used to evaluate all material constants in the constitutive equations investigated.

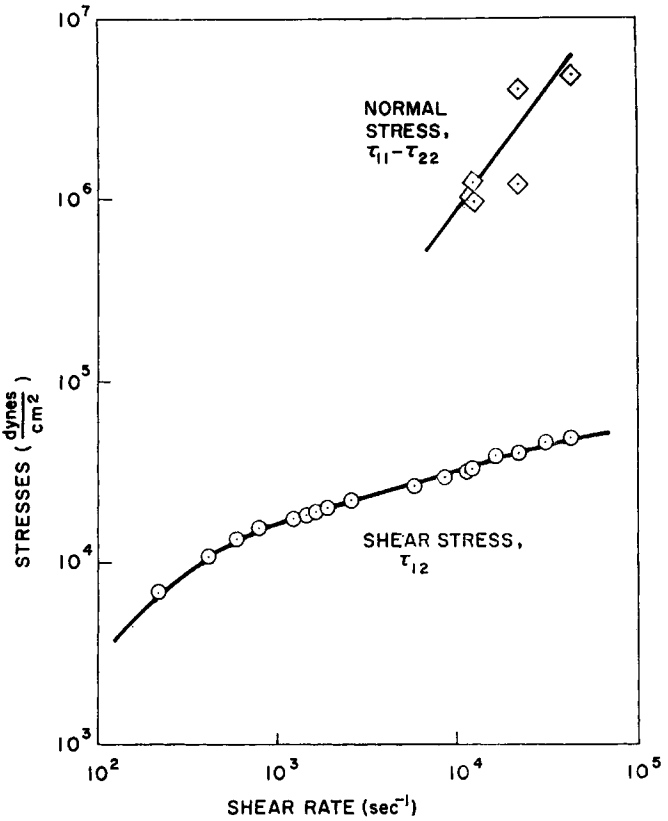

Fig. 15. Shear and normal stresses vs. shear rate for spinning solution.

Table II summarizes various constitutive models—expressions for the shear stress and the normal stress difference and the estimated values of the material constants. It should be mentioned here that the solid line in Figure 16 is equivalent to the viscosity master curve of Graessley,[25] based on a molecular entanglement-network theory, and indicates that the polymer solution is probably of a very narrow molecular weight distribution. Furthermore, this molecular theory gives a molecular relaxation time of 3.6×10^{-3} sec, which is approximately equal to the relaxation times obtained with the continuum models described below.

The material constants for the constitutive theories are estimated by the following method. For each model, a curve of η/η_0 versus $\dot{\gamma}\lambda$ is drawn, where λ is the material (time) constant. Superposing these master curves on Figure 16 enables us to evaluate the numerical value of λ. The values of the material constants obtained for the Oldroyd model were $\lambda_1 = 1.8 \times 10^{-3}$ sec and $\lambda_2 = 2 \times 10^{-4}$ sec, and for the Spriggs model, $\lambda = 1.8 \times 10^{-3}$ sec. From molecular theory one obtains the value 3.6×10^{-3} sec. The orders of magnitude of the time constants are considered to be in fairly good agreement. No value can be obtained from Lodge's model, since his

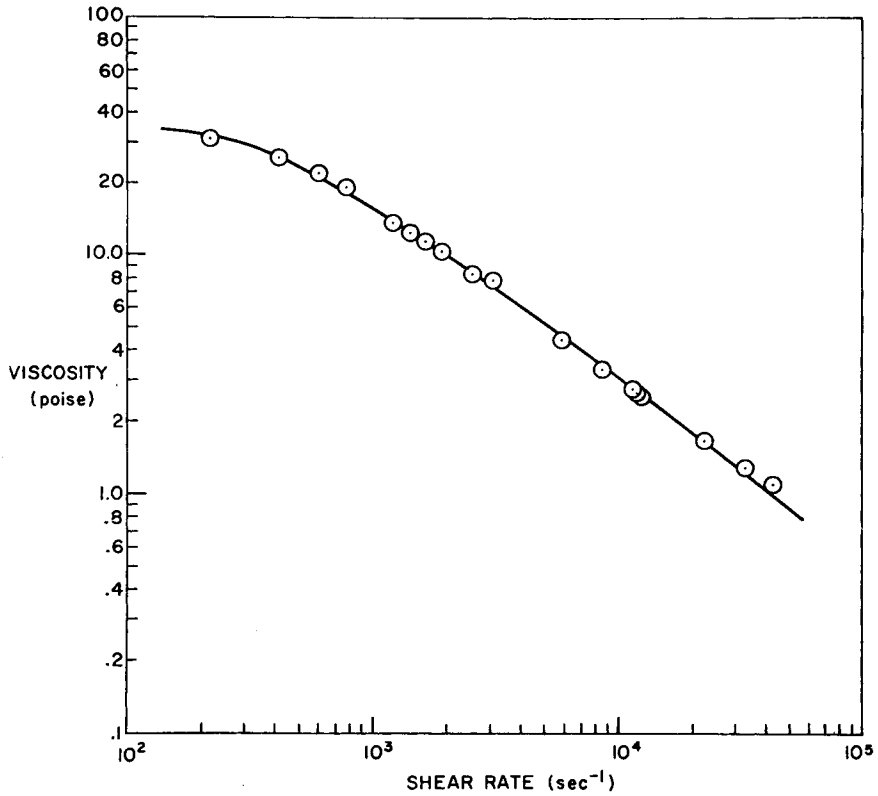

Fig. 16. Shear viscosity vs. shear rate for spinning solution.

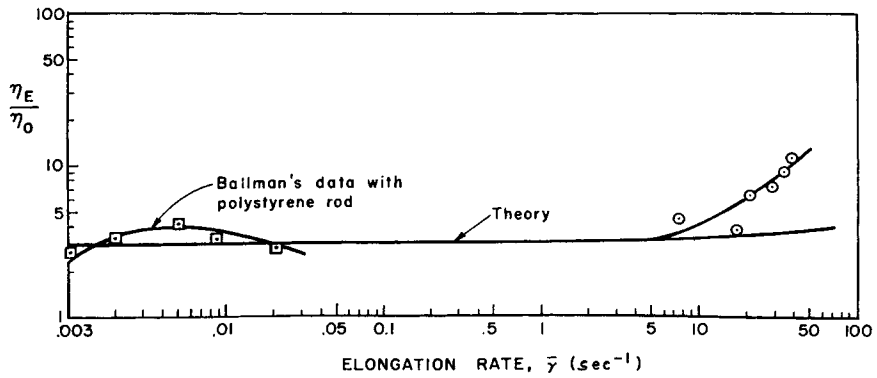

Fig. 17. Comparison between the experimentally obtained and theoretically predicted elongational viscosity. (Circled data points are based on the spinning conditions: bath temp. = 20°C; bath concn. = 20% NaSCN; spinnerette diam. = 0.015 in.)

TABLE II
Evaluation of Time Constants in Various Constitutive Models

Model	Shear stress	Normal stress difference	Elongational viscosity	Material constants[a]
Three-constant Oldroyd model	$\tau_{12} = \frac{\eta_0\dot{\gamma}(1 + {}^2/_3\lambda_1\lambda_2\dot{\gamma}^2)}{(1 + {}^2/_3\lambda_1{}^2\dot{\gamma}^2)}$	$\tau_{11} - \tau_{22} = \frac{2\eta_0(\lambda_1 - \lambda_2)\dot{\gamma}^2}{(1 + {}^2/_3\lambda_1{}^2\dot{\gamma}^2)}$	$\eta_E = \frac{3\eta_0(1 - \lambda_2\bar{\gamma})}{(1 - \lambda_1\bar{\gamma})}$	$\lambda_1 = 1.8 \times 10^{-3}$ sec $\lambda_2 = 2 \times 10^{-4}$ sec
Spriggs model (for $\epsilon = 0$ and $p = 1$)	$\tau_{12} = \frac{\eta_0\dot{\gamma}}{1 + {}^2/_3\lambda^2\dot{\gamma}^2}$	$\tau_{11} - \tau_{22} = \frac{2\eta_0\lambda\dot{\gamma}^2}{1 + {}^2/_3\lambda^2\dot{\gamma}^2}$	$\eta_E = \frac{3\eta_0}{1 - \lambda\bar{\gamma}}$	$\lambda = 1.5 \times 10^{-3}$ sec
Lodge's model	$\tau_{12} = \eta_0\dot{\gamma}$	$\tau_{11} - \tau_{22} = \eta_0\tau_1\dot{\gamma}^2$	$\eta_E = \frac{3\eta_0}{(1 + \tau_1\bar{\gamma})(1 - 2\tau_1\bar{\gamma})}$	...

[a] Note that in all cases $\eta_0 = 33.5$ poises as estimated from Figure 14.

integral theory predicts a constant shear viscosity. It must be noted that the two continuum models correlated reasonably well with the true behavior near the transition region of viscosity, but did not correlate well (in fact, very poorly) at high shear rates (say, above $\dot{\gamma} = 1000\ \text{sec}^{-1}$).

Figure 17, a summary of theoretical and experimental results, indicates that the constitutive theories are potentially useful in describing the observed elongational behavior. It should be recalled here that the spinning data of the present study represents a situation of minimum physically realizable hardening for the system chosen, i.e., with bath concentration of 20% NaSCN and no temperature differential. As such, the magnitude of the experimentally determined elongational viscosity would be higher than that which might be expected if hardening is completely eliminated. Therefore, the difference in magnitude between the experimental and the theoretical curves (which is not great, but significant) may be attributable to the fact that the experiment has not met the condition of complete freedom from the influence of hardening. Also, the particular shape of the experimentally determined elongational viscosity curves may be equally dependent on the hardening process. Thus, the theoretical curves may be considered to be reasonable in predicting the elongational viscosity in the ideal case of "no hardening," but should be modified to account for the real wet-spinning process where hardening occurs.

The maximum rate of elongation encountered in our wet-spinning experiments is approximately $10^2\ \text{sec}^{-1}$. Below this value, all the constitutive theories discussed above predict an elongational viscosity which is virtually independent of rate of elongation, that is, the Trouton viscosity, $3\eta_0$. This predicted behavior has come from the small magnitude of the time constants of the fluid dealt with. At higher elongation rates, the constitutive theories predict that the elongational viscosity increases indefinitely, but it is clear that this behavior would not be realizable in practice. For example, for a fluid with a time constant of 10^{-3} sec, an elongation rate of $10^4\ \text{sec}^{-1}$ must be approached before the elongational viscosity becomes 10 times the Newtonian viscosity. This is physically impossible, since breakage would probably occur before such a high elongation rate is applied. Thus, while the constitutive theories discussed here do predict that the elongational viscosity increases with elongation rate, quantitative correlation between experimental and theoretical curves is not apparent.

CONCLUSIONS

Polyacrylonitrile fibers are wet spun in order to experimentally determine the elongational viscosity. The magnitude of the experimentally determined elongational viscosity is a little higher than that of the theoretically predicted one, which may be attributable to the fact that the experiment has not met the condition of complete freedom from the

influence of coagulation. Therefore the magnitude of the experimentally determined elongational viscosity would be higher than that which might be obtained if hardening is completely eliminated. In light of this consideration, the present study indicates that the dependence of elongational viscosity on rate of elongation is rather weak, and for practical purposes one may consider the elongational viscosity independent of rate of elongation. It is further found that in wet spinning the influence of coagulation (due to mass and heat transfer) on elongational viscosity is far more important than the rate of elongation.

The work was supported in part by a grant from Solvay et Cie, for which the authors are grateful. The authors also wish to thank Drs. D. J. Johnson and S. N. Chinai of American Cyanamid Company who kindly supplied the authors with a large quantity of the materials for the spinning experiments.

References

1. H. S. Nitschmann and J. Schrade, *Helv. Chim. Acta*, **31**, 297 (1948).
2. F. T. Trouton, *Proc. Roy. Soc.*, **77**, 426 (1906).
3. R. L. Ballman, *Rheol. Acta*, **4**, 137 (1965).
4. V. A. Kargin and T. I. Sogolova, *Zh. Fiz. Khim.*, **23**, 540 (1949); *ibid.*, **23**, 551 (1949).
5. B. V. Radyshkevich, V. D. Fixman, and G. B. Vinogradov, *Dokl. Akad. Nauk*, **180**, 404 (1968).
6. A. Ziabicki and K. Kedzierska, *J. Appl. Polym. Sci.*, **2**, 14 (1959); *ibid.*, **6**, 111 (1962).
7. A. Ziabicki, *Kolloid-Z. Z. Polymer*, **175**, 14 (1961).
8. A. Ziabicki and K. Kedzierska, *Kolloid-Z. Z. Polym.*, **171**, 151 (1960).
9. M. Yamamoto, *J. Phys. Soc. Jap.*, **12**, 1148 (1957).
10. A. S. Lodge, *Elastic Liquids*, Academic Press, New York, 1964.
11. J. L. White, *J. Appl. Polym. Sci.*, **8**, 1129 (1964).
12. R. Roscoe, *Brit. J. Appl. Phys.*, **16**, 1567 (1965).
13. W. Noll, *Arch. Ratl. Mech., Anal.*, **2**, 197 (1958).
14. B. D. Coleman and W. Noll, *Ann. N. Y. Acad. Sci.*, **89**, 715 (1961).
15. R. B. Bird and T. W. Spriggs, *Phys. Fluids*, **8**, 1390 (1965).
16. M. C. Williams and R. B. Bird, *Phys. Fluids*, **5**, 1126 (1962).
17. T. W. Spriggs, *Chem. Eng. Sci.*, **20**, 931 (1965).
18. R. B. Bird, M. W. Johnson, and J. F. Stevenson, paper presented at the Fifth International Congress on Rheology, Kyoto, Japan, October 1968.
19. R. I. Tanner and J. M. Simmons, *Chem. Eng. Sci.*, **22**, 1803 (1967).
20. B. C. Shertzer, Ph.D. Dissertation, University of Delaware, Newark, Delaware, 1965.
21. R. M. Griffith, *Ind. Eng. Chem., Fund.*, **3**, 245 (1964).
22. H. F. Mark, E. Cernia, and S. Atlas, *Man Made Fibers*, Wiley, New York, 1967.
23. D. R. Paul, *J. Appl. Polym. Sci.*, **12**, 383 (1968).
24. D. R. Paul, *J. Appl. Polym. Sci.*, **12**, 2273 (1968).
25. W. W. Graessley, *J. Chem. Phys.*, **43**, 2696 (1965).

Received May 4, 1970